IEEE Access
Multidisciplinary | Rapid Review | Open Access Journal

Received November 3, 2020, accepted November 18, 2020, date of publication November 30, 2020,
date of current version December 11, 2020.

Digital Object Identifier 10.1109/ACCESS.2020.3041310

A MRAS Based Model Predictive Control for Multi-Leg Based Multi-Drive System Used in Hot Rolling Mill Applications

MEHDI SAFAEIAN, ABOLFAZL JALILVAND, (Member, IEEE), AND ASGHAR TAHERI, (Member, IEEE)
Department of Electrical Engineering, University of Zanjan, Zanjan 45371-38791, Iran
Corresponding author: Asghar Taheri (taheri@znu.ac.ir)

ABSTRACT In this paper, a multi-leg based multi-drive configuration is presented to be used in multi AC drive applications such as the hot rolling mills. The proposed configuration enjoys compactness, fewer semiconductors, and lower drive cost compared with conventional topology, making it a promising approach. In a conventional rolling mill stand, an active front-end (AFE) rectifier and two inverters are required for grid-side and motor-side connections. However, in the proposed configuration, all converters are unified using a multi-leg structure. To improve the operational performance of the drive, a model predictive control (MPC) is designed. In this approach, an individual cost function for every output, along with a comprehensive cost function containing all control objectives for the overall system, is defined. By obtaining the valid and invalid switching states of the proposed converter, the defined multi-objective cost function is minimized to find the most optimum switching states in each sampling time. In addition, to improve the robustness of the proposed multi-drive system, a model reference adaptive system (MRAS) is designed to estimate rotor speed and stator resistance. The high-performance capability of the proposed multi-drive system is evaluated in both steady and dynamic states using MATLAB/Simulink software and compared with a conventional configuration. According to simulation results, it is deduced that the independent control of the top and bottom motors in a rolling mill stand can be guaranteed using the proposed low-cost sensor-less drive.

INDEX TERMS Cost function, induction motor, model predictive control, robustness, model reference adaptive system, multi-drive system, rolling mill.

NOMENCLATURE

$\vec{i}_g = i_{g\alpha} + ji_{g\beta}$	grid-side current vector
$\vec{v}_g = v_{g\alpha} + jv_{g\beta}$	grid-side voltage vector
$\vec{v}_{afe} = v_\alpha + jv_\beta$	voltage vector generated by grid-side converter
R_g, L_g	grid-side resistance and filter inductance
T_s	sampling time
$P(k+1)$, $Q(k+1)$	predicted active and reactive power of the grid-side
L_m	mutual inductance
R_s, L_s	stator resistance and inductance
R_r, L_r	rotor resistance and inductance
$\vec{i}_s$	stator current vector
$\vec{v}_s$	stator voltage vector
$\vec{i}_r$	rotor current vector
$\vec{\psi}_s$	stator flux vector
$\vec{\psi}_r$	rotor flux vector
T_e	developed electromechanical torque
p	number of pole pairs
ω	rotor electrical speed
$\sigma = 1 - L_m^2/L_sL_r$	leakage factor
$\tau_r = L_r/R_r$	rotor time constant
$k_r = L_m/L_r$	rotor coupling factor
$R_\sigma = R_s + k_r^2 R_r$	equivalent resistance
$\tau_\sigma = \sigma L_s/R_\sigma$	equivalent time constant
$P^\star$, $Q^\star$	grid-side active and reactive power references
J_G	grid-side port cost function
$T_e^\star$	torque reference

The associate editor coordinating the review of this manuscript and approving it for publication was Huiqing Wen.

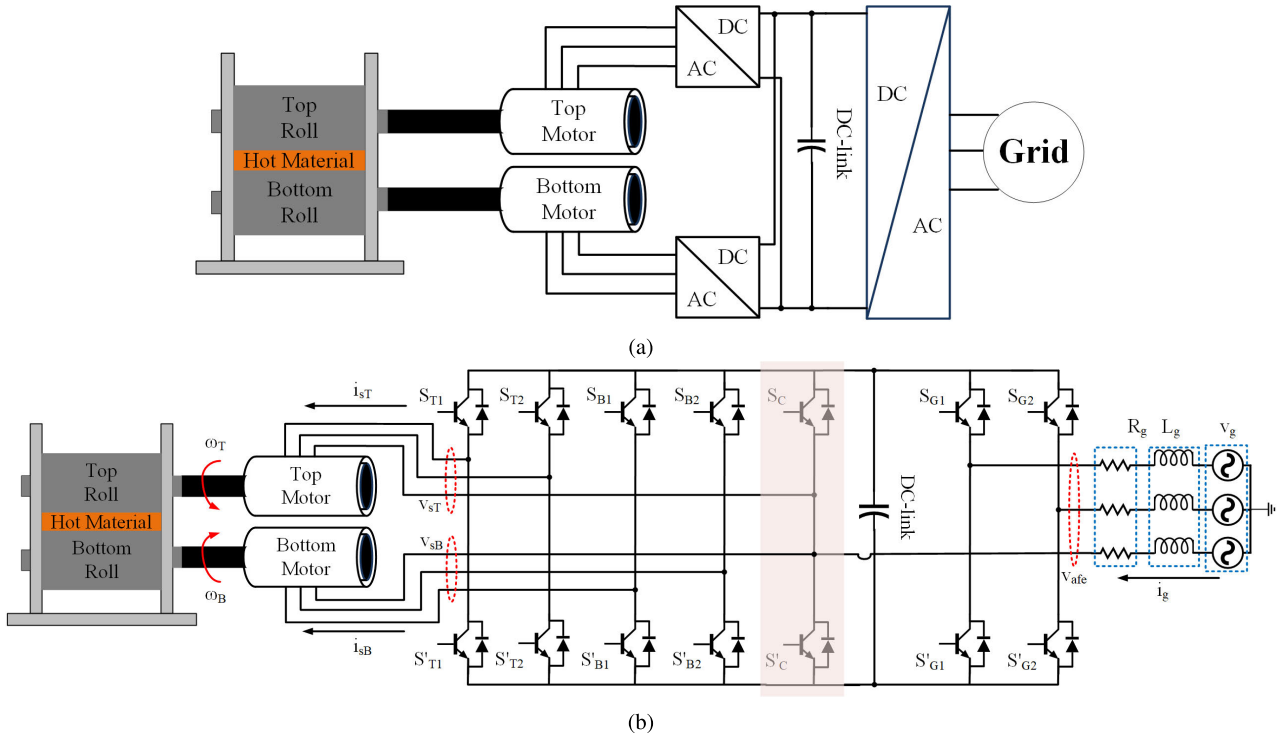

FIGURE 1. Hot rolling mills configuration, (a) conventional back-to-back structure, and (b) proposed multi-leg structure.

$\psi_s^\star$	stator flux reference
J_M	motor-side port cost function
λ_M	motor-side weighting factor
λ	weighting factor
J_T	total cost function
$\hat{\psi}_{rI}$	Estimated rotor flux by adaptive model
$\hat{\psi}_r$	Estimated rotor flux by reference model
$\hat{R}_s, \hat{R}_r$	Estimated stator and rotor resistance

I. INTRODUCTION

Over the last two decades, the induction motor (IM) based adjustable speed drives (ASDs) have regularly experienced significant developments, particularly in their control system [1], [2]. The rolling mill is one of the most demanding applications for IM based ASDs, which needs a precise speed and torque control. A hot rolling mill includes several rolling stands in which each stand contains a top and a bottom roll mechanically linked to an electric motor [3]. Most conventional rolling mills are based on DC drives in which two DC motors are controlled using two DC-DC converters. However, due to the advantages of the AC drives, including more efficiency and lower maintenance cost compared with DC drives, using AC drives in recently installed rolling mills and also replacing them with DC drives have to be taken into consideration. It is worth mentioning that since all installed drives in the rolling train need to have the same operating characteristic, replacing AC drives with the existing DC drives can be a remarkable challenge [4].

In a conventional AC drive based rolling mill stand, the top and bottom electric motors are controlled using individual inverters as shown in Fig. 1(a). These inverters are electrically linked through a DC-link capacitor and convert the DC voltage to a controllable AC voltage, delivering active and reactive powers to the motors in different operating points. To regulate the DC-link voltage, a grid-side converter working as an active front-end (AFE) rectifier is also needed. This AFE rectifier is responsible for delivering a sufficient amount of power to DC-link depending on the motors' operating characteristics.

Different grid and motor-side converters are presented in the literature for being used in a hot rolling mill stand [5]–[11]. In [5], considering the drawbacks of the DC drives, a line-commutated cyclo-converter based AC drive is reported. Despite the high number of thyristors needed for its implementation, it provides the imperative dynamic response required in rolling mill applications properly. The power quality problems of an actual cyclo-converter based hot rolling train, including roughing and finishing mills, is relieved using a cascaded H-bridge based static compensator (STATCOM) [6], [7]. The reactive power management to achieve unity power factor in the grid side and harmonic elimination from grid-side current are the most important power quality issues considered in [7]. It is worth mentioning that milling steel's characteristics and the rolling train are considered in designing the STATCOM. To improve the power quality issues in the grid side through a proper active and reactive power flow management without using an individual STATCOM, three cyclo-converters installed in the

finishing rolling mill of the same hot rolling train are replaced by three-level based back-to-back (BtB) converters [8]. In addition to the harmonic distortion improvement in the grid side because of using a three-level converter, the installation cost of additional STATCOM for power quality improvement can be omitted. In [9], [10], the principles of selecting and designing the high-reliability converters for both grid and motor sides are presented. For this aim, an actual 7 MW hot rolling mill installed in southeastern Brazil is analyzed. In the existing version, a BtB neutral-point-clamped (NPC) is used for the grid and motor sides. However, considering the reliability criteria for the selection of converters, a fault-tolerant version of the active NPC converter (FT-NPC) and the triple-star bridge cells modular multilevel converter (TSBC-MMC) are presented and compared. In term of the installation cost, the FT-NPC is the better one, however, the TSBC-MMC enjoys lower electric loss and better surviving from the faults. A three-level gate-turn-off thyristor (GTO) voltage source based converter for the grid and motor sides, which offers a fast torque response time, is also presented in [11].

As it is observed in Fig. 1(a), three individual converters are required in a conventional hot rolling mill stand, which yields a significant increase in the required AC drive's cost. The multi-port converters with the capability of handling different AC outputs offering a lower number of semiconductors are recently reported in the literature in various applications, including the integration of the renewable energy sources (RES) [12], [13], hybrid electric vehicle (HEV) [14], and uninterruptible power supplies (UPSs) [15]. The multi-leg converter is one of the most promising unified converters in which a leg is shared between different outputs [16]. The five-leg version of this unified converter is used in different applications including multi-phase motor [17], multi-drive system [18], and unified power quality conditioner (UPQC) [19]. In [20] a five-leg converter is reported to be replaced with the back-to-back converter in ASDs. During the fault in one leg of the BtB converter, the BtB converter is reconfigured as a five-leg converter in which the active front-end and motor side converters are shared in a leg. The reconfigured structure can follow the pre-given reference values in both the grid and motor sides.

In this paper, to reduce the drive's cost of a conventional rolling mill stand, a multi-leg based multi-drive configuration is presented, as shown in Fig. 2(b). The proposed converter offers a unified configuration for integrating all grid-side and motor-side converter, leading to fewer required semiconductors, hence lower drive's cost. Compared with the five-leg converter presented in [20], which can only interconnect a motor with the grid, the proposed configuration can integrate both top and bottom motors to the grid. Besides, considering control objectives for motors and grid, a modified MRAS based MPC approach for independent control of induction motors (IMs) and the grid is developed, which is another salient feature of this paper.

TABLE 1. Feasible switching states and generated vectors of a three-phase three-leg converter.

Vector Number	Switching State	Generated Vector
v_0	000	0
v_1	100	$2/3v_{dc}$
v_2	110	$1/3v_{dc} + j\sqrt{3}/3v_{dc}$
v_3	010	$-1/3v_{dc} + j\sqrt{3}/3v_{dc}$
v_4	011	$-2/3v_{dc}$
v_5	001	$-1/3v_{dc} - j\sqrt{3}/3v_{dc}$
v_6	101	$1/3v_{dc} - j\sqrt{3}/3v_{dc}$
v_7	111	0

II. MODELING OF THE MULTI-LEG BASED MULTI-DRIVE

In the multi-leg-based multi-drive system presented in this paper, one output is used to be connected to the grid, which is responsible for supporting DC-link and therefore providing the requested active and reactive power by IMs. Other outputs, responsible for delivering requested active and reactive power to IMs so that their speed references can be appropriately tracked, are connected to IMs. As it is shown in Fig. 1(b), all outputs are shared in one leg of the multi-leg converter (switch S_{C1} and S_{C2}). This shared leg yields a 22% reduction in the number of required semiconductors for a rolling mill stand compared with the conventional BtB structure shown in Fig. 1(a). However, the autonomous control of outputs is affected and would be a remarkable challenge in the proposed configuration. To handle this challenge, a modified MPC is developed for the proposed configuration considering all control objectives.

The grid-side converter, containing leg S_{G1}, leg S_{G2}, and shared leg, is considered as a three-phase active front-end (AFE) rectifier. The top motor's converter, comprised of leg S_{T1}, leg S_{T2}, shared leg and the bottom motor's converter, comprised of leg S_{B1}, leg S_{B2}, shared leg, treat as three-phase inverters. To design the model predictive control for the proposed multi-leg-based multi-drive configuration, it is essential to model different parts of the proposed configuration, as given in the following section.

A. MULTI-LEG CONVERTER MODEL

In this paper, the proposed multi-leg converter is considered an ideal converter in which the semiconductors have no voltage drop and delay time. Considering these assumptions, the switching state of every leg in the proposed multi-leg converter can be defined as follows [20]:

$$S_j = \begin{cases} 1 & \text{if the first switch in the } j^{th} \text{ leg is ON} \\ 0 & \text{if the second switch in the } j^{th} \text{ leg is OFF} \end{cases} \quad (1)$$

where j can be 1 to 7 for the proposed configuration. It is noted that this study uses the equations presented by Zhou *et al.* [20] for modeling both grid-side and motor-side converters.

As the grid-side rectifier and motor-side inverters (considering the shared leg) can be a three-phase three-leg converter, the number of required switching states for covering all possible vectors in these converters is the same and equal to 8. As expressed in Table 1, six active and two zero vectors can be

TABLE 2. Feasible switching states of a five-leg converter.

Output Vectors		Switching State				
First Vector	Second Vector	S_{T1}	S_{T2}	S_{G1}	S_{G2}	S_{C1}
v_0	v_0	0	0	0	0	0
v_0	v_3	0	0	0	1	0
v_0	v_1	0	0	1	0	0
v_0	v_2	0	0	1	1	0
v_3	v_0	0	1	0	0	0
v_3	v_3	0	1	0	1	0
v_3	v_1	0	1	1	0	0
v_3	v_2	0	1	1	1	0
v_1	v_0	1	0	0	0	0
v_1	v_3	1	0	0	1	0
v_1	v_1	1	0	1	0	0
v_1	v_2	1	0	1	1	0
v_2	v_0	1	1	0	0	0
v_2	v_3	1	1	0	1	0
v_2	v_1	1	1	1	0	0
v_2	v_2	1	1	1	1	0
v_5	v_5	0	0	0	0	1
v_5	v_4	0	0	0	1	1
v_5	v_6	0	0	1	0	1
v_5	v_7	0	0	1	1	1
v_4	v_5	0	1	0	0	1
v_4	v_4	0	1	0	1	1
v_4	v_6	0	1	1	0	1
v_4	v_0	0	1	1	1	1
v_6	v_5	1	0	0	0	1
v_6	v_4	1	0	0	1	1
v_6	v_6	1	0	1	0	1
v_6	v_7	1	0	1	1	1
v_7	v_5	1	1	0	0	1
v_7	v_4	1	1	0	1	1
v_7	v_6	1	1	1	0	1
v_7	v_7	1	1	1	1	1

defined considering these switching states. These switching vectors are not individually valid and need to be considered simultaneously with switching vectors of other outputs due to sharing a leg between grid- and motor-side converters. For the sake of clarity, the valid switching states for a five-leg version of the proposed multi-leg converter (eliminating legs S_{B1} and S_{B2} from Fig. 1(b)) are summarized in Table 2. As can be seen, the vector corresponding to each switching state affects all outputs simultaneously, which means independent control of the outputs might deteriorate. To avoid this, the sequential space vector modulation (SSVM) is presented in the literature [14]. In the SSVM approach, the individual switching states that are active vectors for one output while simultaneously are zero for others are sequentially used. In this paper, the shared leg state is considered the leading state in selecting procedure of the appropriate switching states to minimize the computational burden of the proposed approach.

B. THREE-PHASE AFE RECTIFIER MODEL

The dynamic model of a three-phase AFE containing a three-phase ideal source, a grid-side resistor, and a grid-side inductance can be written as follows [20]:

$$\frac{d\vec{i}_g(t)}{dt} = -\frac{R_g}{L_g}\vec{i}_g(t) + \frac{1}{L_g}\vec{v}_g(t) - \frac{1}{L_g}\vec{v}_{afe}(t) \tag{2}$$

by discretizing (2), the grid-side current for the next sampling time $(k+1)$ can be predicted as follows:

$$\vec{i}_g(k+1) = (1 - \frac{R_g T_s}{L_g})\vec{i}_g(k) + \frac{T_s}{L_g}\vec{v}_g(k) - \frac{T_s}{L_g}\vec{v}_{afe}(k) \tag{3}$$

As mentioned earlier, the grid-side converter is responsible for DC-link voltage regulation by providing the requested active power by IMs. For this purpose, the grid-side current components in the synchronous reference frame need to be adequately controlled. In the synchronous reference frame, the active power is controlled using the direct component of the grid-side current, while the reactive power is controlled using quadrature component one. The active and reactive powers that need to be delivered to DC-link in the next sampling time can be expressed by:

$$P(k+1) = \Re(\vec{v}_g(k+1)\bar{\vec{i}}_g(k+1)) \tag{4}$$

$$Q(k+1) = \Im(\vec{v}_g(k+1)\bar{\vec{i}}_g(k+1)) \tag{5}$$

It is noted that since the sampling frequency is much higher than the fundamental frequency of the grid, the grid-side voltage can be considered constant.

C. INDUCTION MOTOR MODEL

The main electrical and mechanical dynamic equations of asymmetrical three-phase squirrel-cage IM in the stationary reference frame can be written as follows [20], [21]:

$$0 = R_r\vec{i}_r + \frac{d\vec{\psi}_r}{dt} - j\omega\vec{\psi}_r \tag{6}$$

$$\vec{v}_s = R_s\vec{i}_s + \frac{d\vec{\psi}_s}{dt} \tag{7}$$

$$\vec{\psi}_r = L_m\vec{i}_s + L_r\vec{i}_r \tag{8}$$

$$\vec{\psi}_s = L_s\vec{i}_s + L_m\vec{i}_r \tag{9}$$

$$T_e = \frac{3}{2}p\vec{\psi} \times \vec{i}_s \tag{10}$$

As the stator currents and rotor speed are the only measurable quantities, other variables including stator flux and torque, need to be estimated and predicted, respectively. For this aim, the unmeasurable variables in the equations mentioned above should be written in terms of measurable quantities. The rotor flux can be expressed as follows:

$$\vec{\psi}_r + \tau_r\frac{d\vec{\psi}_r}{dt} = L_m\vec{i}_s + j\omega\tau_r\vec{\psi}_r \tag{11}$$

Then the stator flux can be estimated using the following equation:

$$\vec{\psi}_s = \frac{L_m}{L_r}\vec{\psi}_r + \sigma L_s\vec{i}_s \tag{12}$$

Considering the stator flux and torque as control variables, the predicted values of these parameters in the next sampling time are needed to optimize the switching states of the motor-side converters. According to (7) and by discretizing, the stator flux is predicted as follows [20]:

$$\vec{\psi}_s(k+1) = \vec{\psi}_s(k) + T_s\vec{v}_s(k) - R_sT_s\vec{i}_s(k) \tag{13}$$

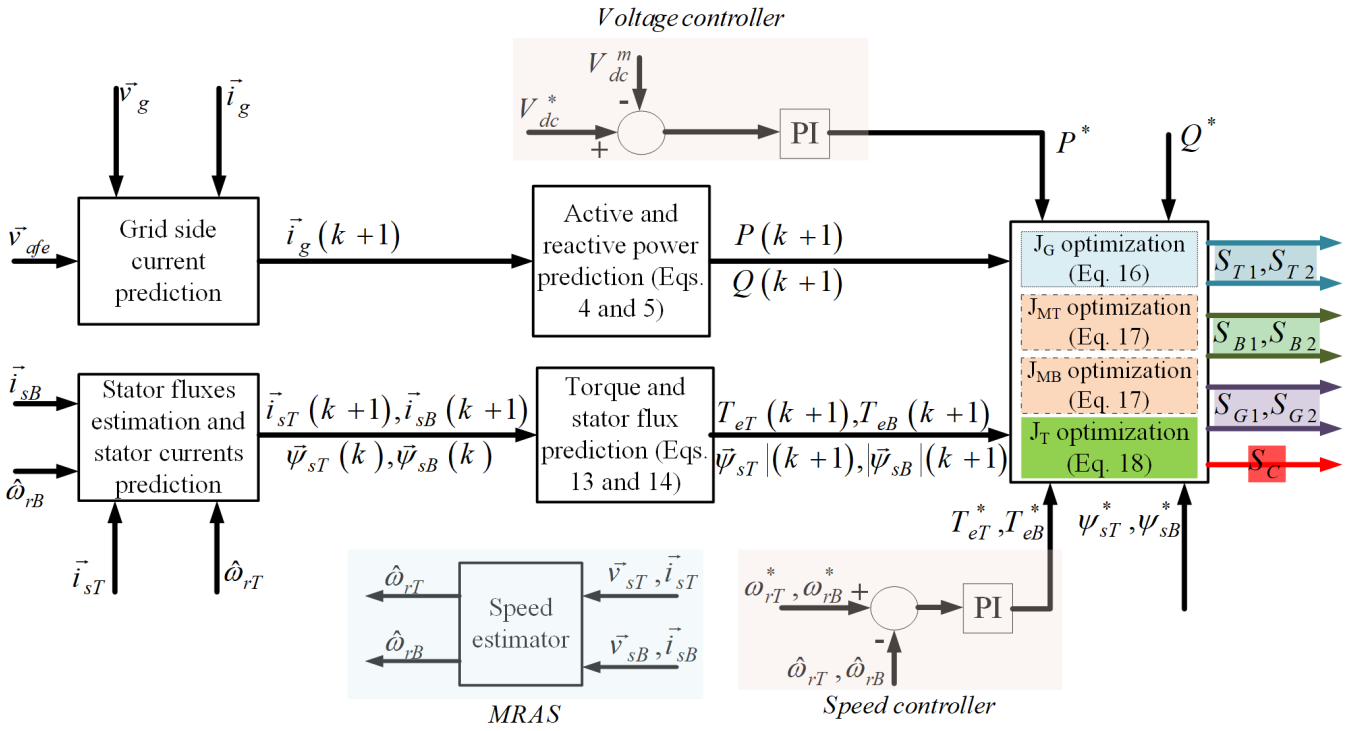

FIGURE 2. MRAS based MPC control designed for multi-leg based multi-drive configuration.

Using the torque equation in the synchronous reference frame and considering the predicted value for the stator flux and the measured value for the stator current, the torque prediction is obtained as follows:

$$T_e(k+1) = \frac{3}{2} p \Im\{\bar{\vec{\psi}}_s(k+1)\vec{i}_s(k+1)\} \tag{14}$$

As can be seen, the stator current prediction in the next sampling time is also needed to predict the torque. Considering equations (6)-(9), the stator current can be predicted by

$$\vec{i}_s(k+1) = (1+\frac{T_s}{\tau_\sigma})\vec{i}_s(k) + \frac{T_s}{T_s+\tau_\sigma}\frac{1}{R_\sigma}((\frac{k_r}{\tau_r} - j\omega(k)k_r)\vec{\psi}_r(k) + \vec{v}_s(k)) \tag{15}$$

III. MPC CONTROL STRATEGY

A. COST FUNCTION DESIGN

In model predictive control, the switching states of a converter are optimized so that the cost function containing the control objectives is minimized. One of the main features of the MPC is its capability in handling multi-objective cost functions. In the proposed multi-leg-based multi-drive system, there are three outputs with different control objectives that need to be met simultaneously. As shown in Fig. 2, the DC-link voltage regulation is the main objective of the grid-side port. For this aim, the reference value for DC-link voltage is first compared with the measured one. Then, using a proportional-integral (PI) controller, the reference value for active power is obtained. It is noted since the unity power factor in the grid side is a must, the reference value for reactive power is set zero. Delivering zero reactive power to the grid is the second control objective for the grid-side converter. According to these control objectives, the cost function of the grid-side converter can be expressed as follows:

$$J_G = (|P^\star - P(k+1)_i| + |Q^\star - Q(k+1)_i|) \quad i \in \{1,2,3,4;5,6,7,8\} \tag{16}$$

For the motor-side converters, speed control is the main objective. As it is shown in Fig. 2, the speed reference defined by the operator is initially compared with the rotor speed values. Next, using a PI controller, the torque's reference value that needs to be induced at the motor's shaft is calculated. Another objective control for motor-side converters is the following of the reference value for the stator flux. Accordingly, the cost function of the motor-side inverters can be designed as follows:

$$J_{Mj} = (|T^\star_{ej} - T_{ej}(k+1)_i| + \lambda_{Mj}||\psi^\star_{sj}| - |\vec{\psi}_{sj}(k+1)_i||) \quad i \in \{1,2,3,4;5,6,7,8\} \quad j \in \{T,B\} \tag{17}$$

where λ_{Mj} is a weighting factor to determine the priority of cost function in the following reference values for torque and stator flux. This factor is considered equal to one in this paper.

Finally, the total cost function of the proposed configuration can be expressed by

$$J_{Tk} = (J_{Gk} + \lambda \sum_{j=T,B} J_{Mk}) \quad k \in \{0,1\} \tag{18}$$

where J_{Tk} is the cost function while the switching state of the common leg is k. λ is also a weighting factor to determine the controller's priority in following the reference values of the grid-side or motor-side converters. Since both grid and motor-side variables have the same importance in this paper, this weighting factor is also set to one.

B. MODIFIED MPC IMPLEMENTATION

In the conventional MPC for a three-phase three-leg converter, the designed cost function is first minimized by evaluating only eight possible voltage vectors related to the valid switching states. The best switching state with the minimum cost is then selected and finally applied to the converter in the next sampling time. For the proposed multi-leg-based multi-drive configuration, there are 2^n (n is the number of legs) switching states and, therefore, voltage vectors that need to be evaluated in each sampling time. This high number of feasible switching states imposes a significant computational burden on the controller, limiting the usage of the MPC in such applications.

To overcome this issue, a modified MPC with a reduced computational burden is developed. As shown in Table 2, the leading state that needs to be determined first is the state of the common leg. Knowing the common leg state, only four switching states and four voltage vectors for every port are defined. As a result, $4 \times n$ switching states need to be evaluated in every sampling time to find the optimum switching states. This reduction in the number of feasible switching states yields a significant reduction in computational time.

Since there are two switching states for the common leg, different outputs' cost functions need to be optimized twice. For every switching state of the shared leg, the cost function of each port is first evaluated for four feasible voltage vectors considering the predicted variables. Knowing the shared leg's switching state, the total cost function is then evaluated to optimize the switching states of other legs. Finally, the total cost function values for two different switching states of the shared leg are compared, and the optimum switching states for all legs are accordingly determined. The step-by-step procedure of finding the optimum switching states in every sampling time can be written as follows:

1) Consider the S_{C1} OFF
2) For $k = 1$ to 4 (the possible states while S_{C1} is OFF)
   - Optimize J_G to find the best state for S_{G1} and S_{G2}
   - Optimize J_{MT} to find the best state for S_{T1} and S_{T2}
   - Optimize J_{MB} to find the best state for S_{B1} and S_{B2}
   - Calculate J_{T1}
3) Consider the S_{C1} ON
4) For $k = 5$ to 8 (the possible states while S_{C1} is ON)
   - Optimize J_G to find the best state for S_{G1} and S_{G2}
   - Optimize J_{MT} to find the best state for S_{T1} and S_{T2}
   - Optimize J_{MT} to find the best state for S_{B1} and S_{B2}
   - Calculate J_{T2}

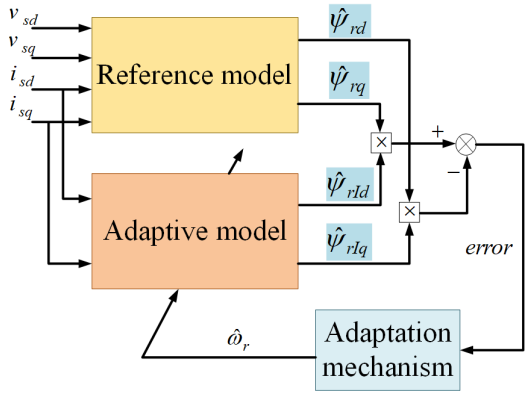

FIGURE 3. MRAS based sensor-less speed estimator.

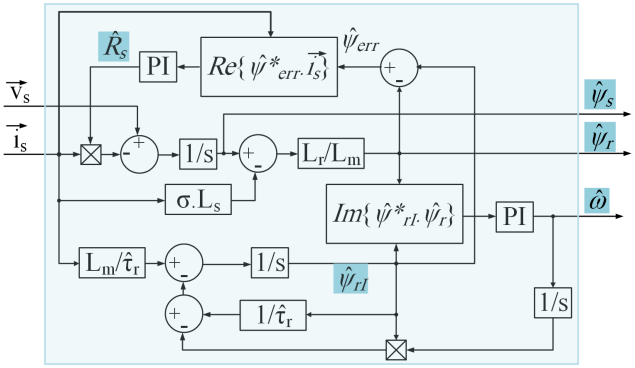

FIGURE 4. Detailed block diagram of the adopted MRAS.

5) If $J_{T1} \leq J_{T2}$
   - Consider S_{C1} OFF and use the optimized states in step 2
6) Otherwise
   - Consider S_{C1} ON and use the optimized states in step 4
7) End

IV. MRAS ESTIMATOR

To provide a sensor-less control for IMs, a model reference adaptive system is used to estimate the rotor speeds. As shown in Fig. 3, in the MRAS approach, two different models, including the reference and adjustable models, are used. The reference model is independent of rotor speed $\hat{\omega}_r$ and uses the measured stator voltage and current in the stationary reference frame to calculate the rotor flux components as follows [22]:

$$\hat{\psi}_s = \int \left(\vec{v}_s - \hat{R}_s.\vec{i}_s\right) dt \tag{19}$$

$$\hat{\psi}_r = \frac{L_r}{L_m}.\left(\hat{\psi}_s - \sigma.L_s.\vec{i}_s\right) \tag{20}$$

In the adaptive model, which is also called the dependent model, the rotor flux components are observed using the measured stator current and estimated rotor speed in the stationary

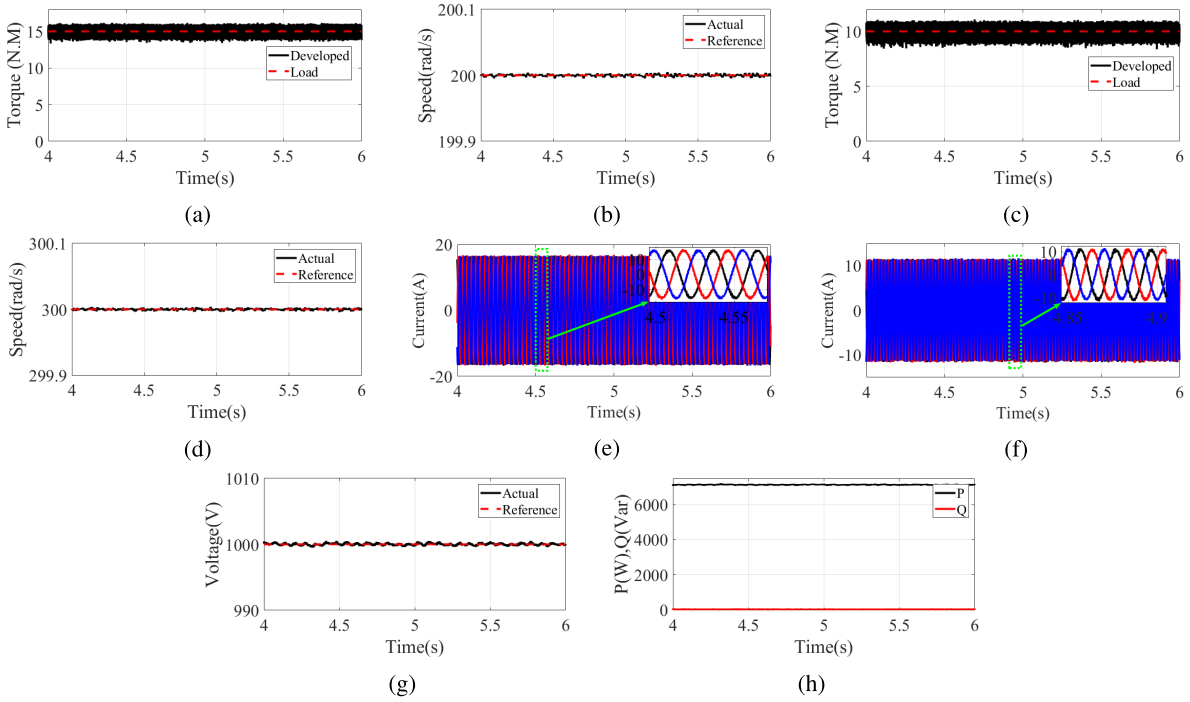

FIGURE 5. Simulation results in steady state without MRAS, (a) first motor torque, (b) first motor speed, (c) second motor torque, (d) second motor speed, (e) stator current of the first motor, (f) stator current of the second motor, (g) DC-link voltage and (b) active and reactive power supplied by the grid.

reference frame as follows:

$$\hat{\psi}_{rI} = \int \left(\frac{L_m}{\hat{\tau}_r} . \vec{i}_s - \left(\frac{1}{\hat{\tau}_r} - j.\hat{\omega}_r \right) . \hat{\psi}_{rI} \right) dt \tag{21}$$

Then, the rotor flux error between the adaptive and reference models is obtained by:

$$e_{\omega_r} = \Im\{\hat{\psi}^{\star}_{rI} . \hat{\psi}_r\} \tag{22}$$

Finally, a conventional PI-controller is utilized to find the estimated rotor speed so that the error mentioned above is forced to zero.

$$\hat{\omega}_r = K_{p\omega} . e_{\omega_r} + K_{i\omega} \int e_{\omega_r} dt \tag{23}$$

This estimated speed rotor is then given to the MPC system to create the torque reference required in cost function calculation.

Every motor's stator resistance R_s might vary with temperature. Though the variation is prolonged, the control system's robustness is enhanced by estimating the actual value of R_s. The speed estimation procedure might also be affected by the rotor time constant $\hat{\tau}_r = L_r/\hat{R}_r$. Considering the variation ratio of the stator resistance, the rotor resistance, and therefore, the rotor time constant is adapted. To improve the robustness of the adopted MRAS, a stator resistance estimator is considered as follows [22], [23]:

$$e_{Rs} = \Re\{(\hat{\psi}_{rI} - \hat{\psi}_r)^{\star} . \vec{i}_s\} \tag{24}$$

$$\hat{R}_s = K_{pRs} . e_{Rs} + K_{iRs} \int e_{Rs} dt \tag{25}$$

The detailed scheme of the adopted MRAS estimator, considering both speed and resistance adaptions, is depicted in Fig. 4.

V. RESULTS AND DISCUSSION

A. STEADY STATE PERFORMANCE

In order to show the proper performance of the proposed MPC based multi-drive configuration, different loads are applied to the IMs considering different speed references in two operating modes: a) without MRAS and b) with MRAS. Fig. 5 and Fig. 6 show the simulation results for the first and second modes, respectively. Fig. 5 (c)-(d) and Fig. 5 (e)-(f) demonstrate the torque and speed for the first and second IM connected to the multi-leg converter, respectively. As it can be deduced, the proposed MPC-based configuration can provide the reference voltages in motor-s-de ports so that the motors can follow their speed references and develop the required electromechanical torques to meet the applied loads. As depicted in Fig. 5 (g)-(h), the stator current of both IMs are sinusoidal with low total harmonic distortion. As shown in Fig. 5(a), the grid-side port can appropriately regulate DC-link voltage, which means the cost function of the grid-side port is accurately optimized. Fig. 5(b) shows the provided active and reactive power by the grid to supply the DC-link, and therefore the induction motors. As can be seen, the unity power factor is also achieved using the proposed control system.

Fig. 6 shows the simulation results when the MRAS is in use for rotor speed estimation. The torque and speed for

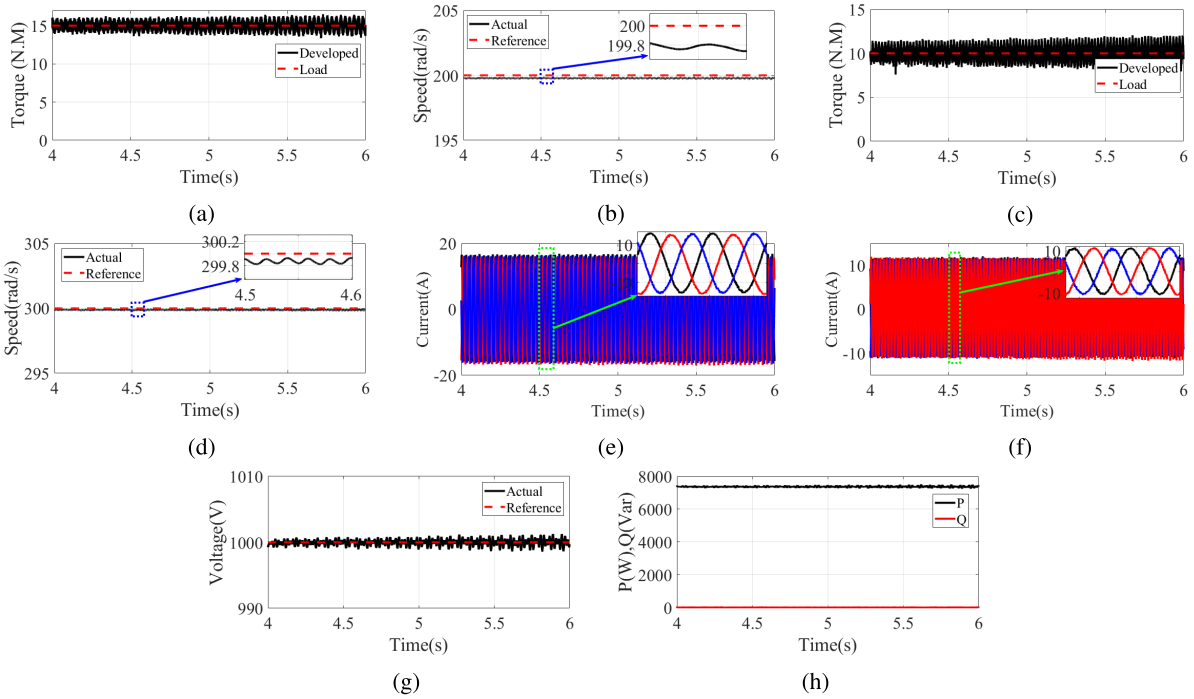

FIGURE 6. Simulation results in steady state with MRAS, (a) first motor torque, (b) first motor speed, (c) second motor torque, (d) second motor speed, (e) stator current of the first motor, (f) stator current of the second motor, (g) DC-link voltage and (b) active and reactive power supplied by the grid.

induction motors are shown in Fig. 6 (c)-(d) and (e)-(f), respectively. Using the MRAS method for rotor speed estimation does not deteriorate the performance of the IMs. In this case, the speed deviations are 0.1% and 0.067% for the first and second IMs, respectively. The stator currents are also shown in Fig. 6 (g)-(h). As it is obvious, the MRAS approach does not have any undesired effect on the stator currents. The DC-link voltage and active and reactive power provided by the grid are shown in Fig. 6 (a)-(b).

According to simulation results in steady-state, it is deduced that the proposed MPC based multi-leg multi-drive configuration can correctly generate the optimum signal gates so that the given reference values can be easily followed.

B. DYNAMIC PERFORMANCE

The dynamic performance of the proposed MPC-based multi-leg multi-drive configuration is also evaluated by applying different step loads to the IMs for both modes including: a) with MRAS (Fig. 7) and b) with MRAS (Fig. 8).

The torque response along with speed variation for the first and second IMs are shown in Fig. 7 (a)-(b) and (c)-(d), respectively. Both motors are effectively able to reach the speed reference in less than one second. As can be seen, the rise time and the overshoot of motors' speed are also acceptable. Besides, when the load changes are applied, the proposed drive can control motors so that they can follow the load changes while the rotor speeds maintain constant. The stator currents of the IMs are illustrated in Fig. 7 (e)-(f). As can be seen, the currents injected into the stator windings are appropriately tracking the load changes. The DC-link voltage and the active and reactive power provided by the grid are shown in Fig. 7 (g)-(h). As can be seen, the proposed MPC control can regulate DC-link voltage so that the provided active power by the grid is tracking the load changes. The reactive power provided by the grid is zero, which means the unity power factor in the grid side can be achieved.

The simulation results in the dynamic state when the MRAS is in use are depicted in Fig. 8. As presented in Fig. 8(a)-(b) and Fig. 8(c)-(d), both IMs can appropriately respond to the load changes, while the MRAS approach is being used for speed estimation. As it is evident, the speed deviations in both IMs caused by load changes are quickly compensated by injecting more current to the stator windings, as shown in Fig. 8(e)-(f). As shown in Fig. 8(g), the DC-link voltage is properly regulated in this mode. Caused by the load changes, and therefore, increasing the requested active power by IM, the DC-link voltage experiences two small dips. However, considering the well-designed modified MPC for the grid side port, these dips can be compensated in a few micro-second. The provided active power to compensate for these dips are illustrated in Fig. 8(h). The dynamic results confirm the well-designing of the proposed modified MRAS based MPC for IMs. As it can be deduced, utilizing the MRAS approach does not have any undesired effect on total harmonic distortion.

C. COMPARISON WITH EXISTING CONFIGURATION

To compare the performance of the proposed configuration with existing structures, a conventional topology consisting

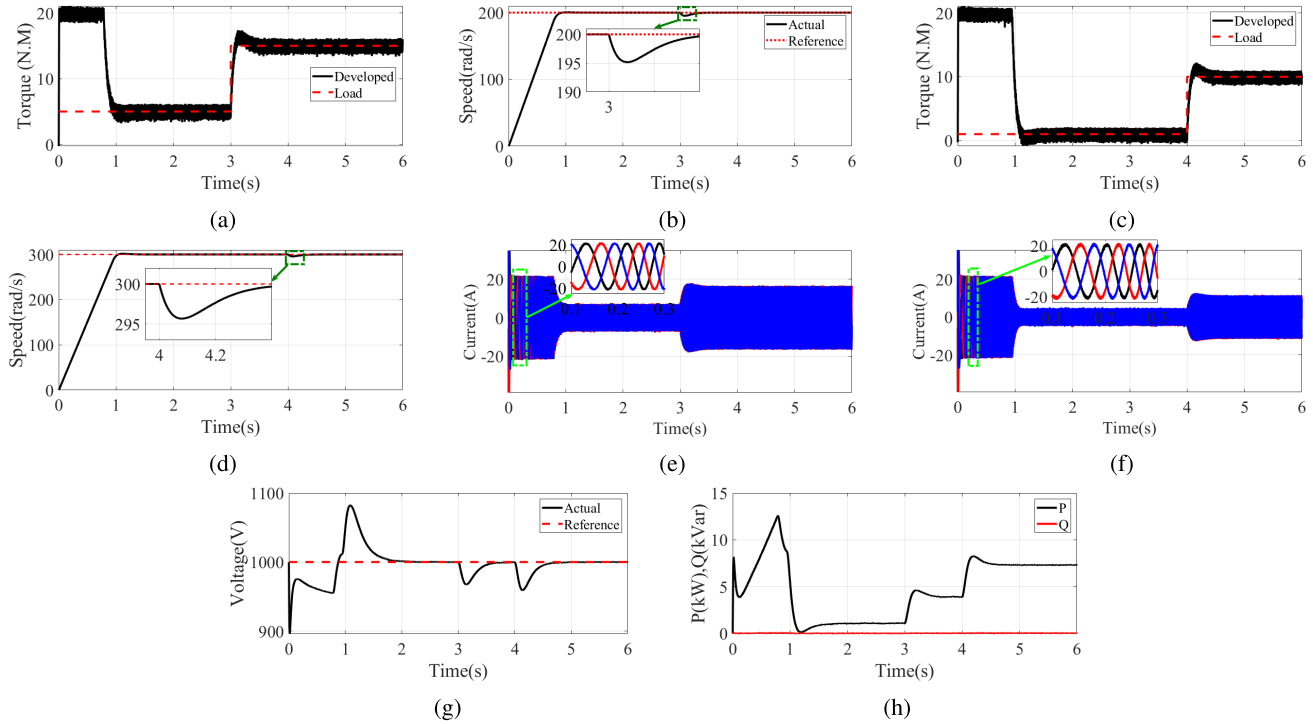

FIGURE 7. Simulation results in dynamic state without MRAS, (a) first motor torque, (b) first motor speed, (c) second motor torque, (d) second motor speed, (e) stator current of the first motor, (f) stator current of the second motor, (g) DC-link voltage and (b) active and reactive power supplied by the grid.

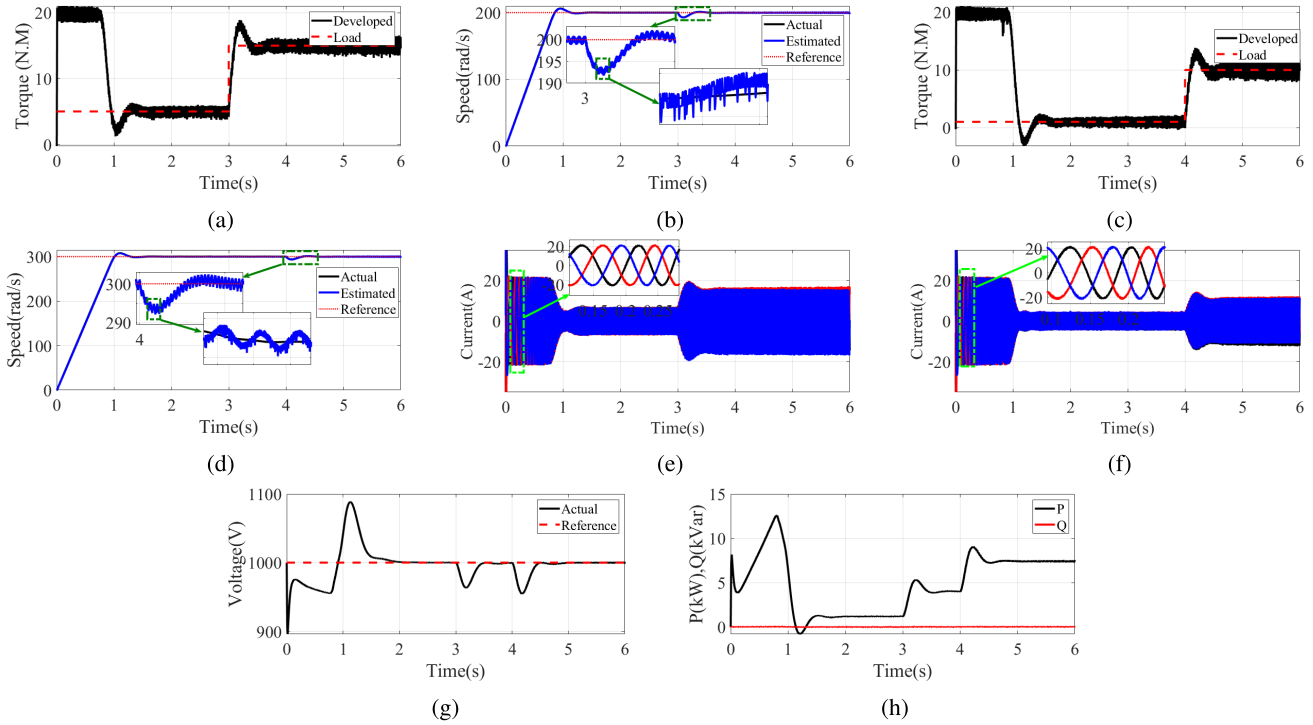

FIGURE 8. Simulation results in dynamic state with MRAS, (a) first motor torque, (b) first motor speed, (c) second motor torque, (d) second motor speed, (e) stator current of the first motor, (f) stator current of the second motor, (g) DC-link voltage and (b) active and reactive power supplied by the grid.

of a grid-side and two individual converters for induction motors, as shown in Fig. 1(a), is taken into account. In this topology, all converters are physically independent and have their controllers. Fig. 9 represent the conventional vector

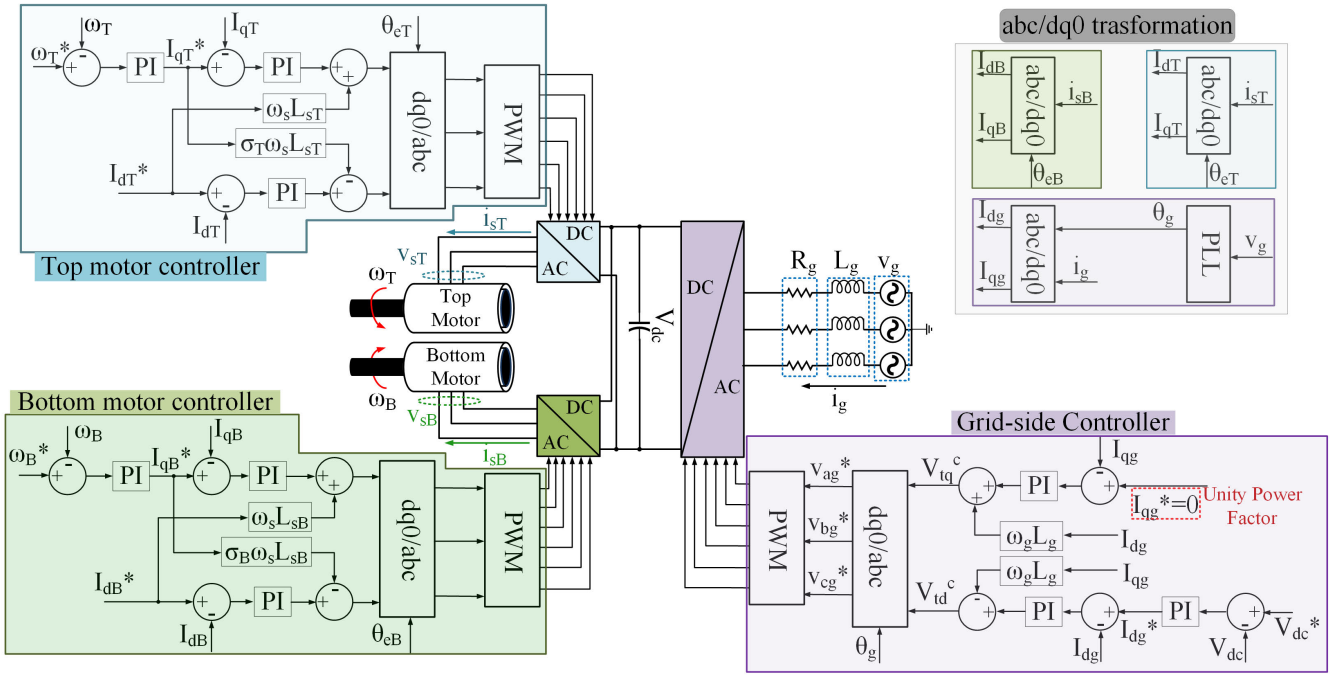

FIGURE 9. Conventional configuration used for comparison.

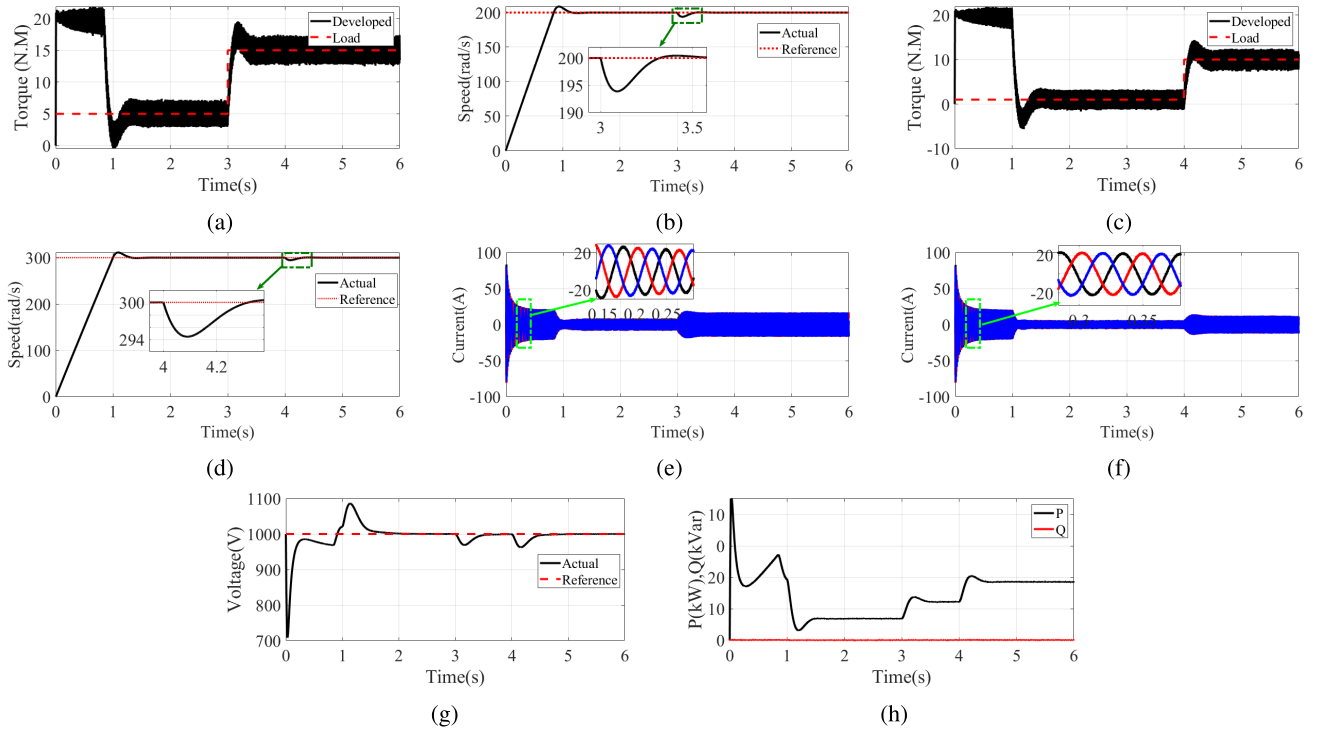

FIGURE 10. Simulation results in dynamic state with conventional configuration, (a) first motor torque, (b) first motor speed, (c) second motor torque, (d) second motor speed, (e) stator current of first motor, (f) stator current of second motor, (g) DC-link voltage and (b) active and reactive power supplied by the grid.

controlled and PQ control strategies for motor-side and grid-side converters. The same loads and speed references as the previous section are applied to the motors for providing a fair comparison. Comparing the results shown in Fig. 10 with Fig. 8 reveals the capability of both configurations in effective control of the motors. In the steady-state mode, using the proposed sensor-less MPC based configuration leads to a lower torque ripple. However, in the transient, the conventional topology offers a lower overshoot in DC-link voltage and motor speed responses.

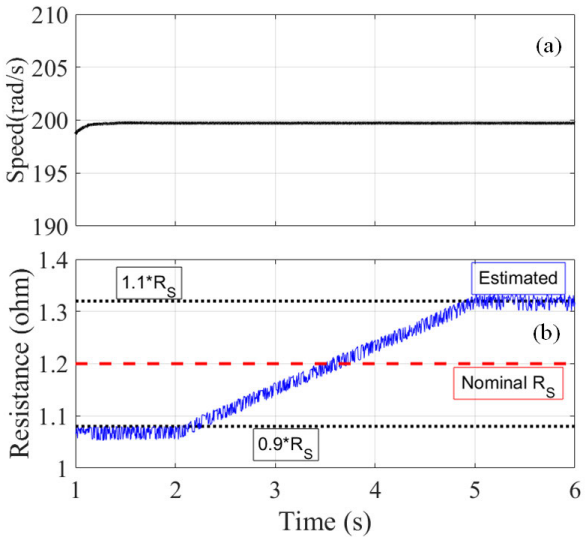

FIGURE 11. Robustness of the configuration considering stator resistance variation.

D. ROBUSTNESS ANALYSIS

To evaluate the robustness of designed MRAS based MPC, the stator resistance variation of the top induction motor is taken into account. For this aim, the stator resistance R_s, which is equal to 1.2 Ω in normal condition, is changed from 1.08 (90% of the normal value) to 1.32 (110 % of the normal value), while the motor operates at 200 rpm speed and 5 N.M load. Fig. 11(a)-(b) demonstrate the motor speed and estimated stator resistance. It can be seen that the system has good robustness concerning stator resistance variation.

VI. CONCLUSION

In this paper, a multi-leg based multi-drive configuration for rolling mill applications is presented to reduce the number of required semiconductors, and therefore, the drive's cost. For this purpose, a stand in the hot rolling process, which conventionally contains a grid side rectifier and two inverters connected to the top and bottom motors, is considered. In the proposed configuration, all grid-side and motor-side converters are replaced with a unified seven-leg converter. A modified MPC with a reduced computational burden is developed for effective control of the induction motors. For this aim, three individual cost functions for the outputs and a total cost function containing all control objectives are designed. By obtaining the valid and invalid switching states of the proposed converter, the defined multi-objective cost function is minimized to find the most optimum switching states in each sampling time. Moreover, to improve the robustness of the proposed MPC based multi-drive system, an MRAS approach is adapted to estimate rotor speed and stator resistance. The simulation results carried out with MATLAB/Simulink software in both steady and dynamic states confirm the ability of the proposed multi-leg based configuration in effective control of the induction motors. The key result of this paper is that the operating requirements of a rolling mill stand can be appropriately met by the proposed multi-leg converter. It can also be deduced from the simulation results that the sensor-less control of the IMs can be guaranteed using the proposed MRAS based MPC without any undesired effect on the performance of the IMs in steady and dynamic states.

REFERENCES

[1] Z. Yang, D. Zhang, X. Sun, and X. Ye, "Adaptive exponential sliding mode control for a bearingless induction motor based on a disturbance observer," *IEEE Access*, vol. 6, pp. 35425–35434, 2018.
[2] N. Farah, M. H. N. Talib, N. S. M. Shah, Q. Abdullah, Z. Ibrahim, J. B. M. Lazi, and A. Jidin, "A novel self-tuning fuzzy logic controller based induction motor drive system: An experimental approach," *IEEE Access*, vol. 7, pp. 68172–68184, 2019.
[3] G. A. Orcajo, J. Rodriguez D., P. Ardura G., J. M. Cano, J. G. Norniella, R. Llera T., and D. Cifrian R., "Dynamic estimation of electrical demand in hot rolling mills," *IEEE Trans. Ind. Appl.*, vol. 52, no. 3, pp. 2714–2723, May 2016.
[4] E. Thorstenson, "Drive selection for rolling mills," *MPT Metall. Plant Technol. Int.*, vol. 32, no. 5, pp. 44–47, 2009.
[5] W. Timpe, "Cycloconverter drives for rolling mills," *IEEE Trans. Ind. Appl.*, vols. IA–18, no. 4, pp. 400–404, Jul. 1982.
[6] G. A. Orcajo, J. M. Cano, J. G. Norniella, F. Pedrayes G., C. H. Rojas, J. Rodriguez D., P. Ardura G., and D. Cifrian R., "Power quality improvement in a hot rolling mill plant using a cascaded H-Bridge STATCOM," in *Proc. IEEE Ind. Appl. Soc. Annu. Meeting*, Sep. 2019, pp. 1–9.
[7] G. A. Alonso Orcajo, J. Rodriguez Diez, J. M. Cano, J. G. Norniella, J. F. Pedrayes, C. H. Rojas, P. Ardura, and D. Cifrian, "Enhancement of power quality in an actual hot rolling mill plant through a STATCOM," *IEEE Trans. Ind. Appl.*, vol. 56, no. 3, pp. 3238–3249, May 2020.
[8] G. Alonso Orcajo, J. Rodriguez D., J. M. Cano, J. G. Norniella, P. Ardura G., R. Llera T., and D. Cifrian R., "Retrofit of a hot rolling mill plant with three-level active front end drives," *IEEE Trans. Ind. Appl.*, vol. 54, no. 3, pp. 2964–2974, May 2018.
[9] V. de Nazareth Ferreira, A. F. Cupertino, H. A. Pereira, A. V. Rocha, S. I. Seleme, and B. de Jesus Cardoso Filho, "Design of high-reliable converters for medium-voltage rolling mills systems," in *Proc. IEEE Ind. Appl. Soc. Annu. Meeting*, Oct. 2017, pp. 1–9.
[10] V. de Nazareth Ferreira, A. F. Cupertino, H. A. Pereira, A. V. Rocha, S. I. Seleme, and B. de Jesus Cardoso Filho, "Design and selection of high reliability converters for mission critical industrial applications: A rolling mill case study," *IEEE Trans. Ind. Appl.*, vol. 54, no. 5, pp. 4938–4947, Sep. 2018.
[11] J. Bocker, J. Janning, and H. Jebenstreit, "High dynamic control of a three-level voltage-source-converter drive for a main strip mill," *IEEE Trans. Ind. Electron.*, vol. 49, no. 5, pp. 1081–1092, Oct. 2002.
[12] H. Bizhani, R. Noroozian, S. M. Muyeen, and F. Blaabjerg, "Wind farm grid integration architecture using unified expandable power converter," *IEEE Trans. Power Electron.*, vol. 34, no. 4, pp. 3407–3417, Apr. 2019.
[13] H. Bizhani, R. Noroozian, S. Muyeen, K. Techato, and F. Blaabjerg, "A grid-connected smart extendable structure for hybrid integration of distributed generations," *IEEE Access*, vol. 7, pp. 105235–105246, 2019.
[14] H. Bizhani, G. Yao, S. Muyeen, S. M. Islam, and L. Ben-Brahim, "Dual mechanical port machine based hybrid electric vehicle using reduced switch converters," *IEEE Access*, vol. 7, pp. 33665–33676, 2019.
[15] C. Liu, B. Wu, N. Zargari, D. Xu, and J. Wang, "Novel nine-switch PWM rectifier-inverter topology for three-phase UPS applications," *EPE J.*, vol. 19, no. 2, pp. 36–44, Jun. 2009.
[16] D. Dujic, M. Jones, S. N. Vukosavic, and E. Levi, "A general PWM method for a $(2n+1)$ -Leg inverter supplying n three-phase machines," *IEEE Trans. Ind. Electron.*, vol. 56, no. 10, pp. 4107–4118, Oct. 2009.
[17] J. A. Riveros, "Pulse width modulation for asymmetrical six-phase machines fed by five-leg converters," in *Proc. 42nd Annu. Conf. IEEE Ind. Electron. Soc.*, Oct. 2016, pp. 5766–5771.
[18] K. Oka and K. Matsuse, "A novel PWM technique with switching-loss reduction for independent drive of two 3-phase AC motors fed by a five-leg inverter," *IEEJ Trans. Electr. Electron. Eng.*, vol. 6, no. 3, pp. 260–265, May 2011.
[19] A. Mannan Rauf, A. Vilas Sant, V. Khadkikar, and H. H. Zeineldin, "A novel ten-switch topology for unified power quality conditioner," *IEEE Trans. Power Electron.*, vol. 31, no. 10, pp. 6937–6946, Oct. 2016.

[20] D. Zhou, J. Zhao, and Y. Li, "Model-predictive control scheme of five-leg AC–DC–AC converter-fed induction motor drive," *IEEE Trans. Ind. Electron.*, vol. 63, no. 7, pp. 4517–4526, Jul. 2016.
[21] J. Rodriguez and P. Cortes, *Predictive Control of Power Converters and Electrical Drives*, vol. 40. Hoboken, NJ, USA: Wiley, 2012.
[22] F. Wang, "Model predictive torque control for electrical drive systems with and without an encoder," Ph.D. dissertation, Dept. Elect. Eng. Inf. Technol., Techn. Univ. München, Munich, Germany, 2014.
[23] V. Vasic, S. N. Vukosavic, and E. Levi, "A stator resistance estimation scheme for speed sensorless rotor flux oriented induction motor drives," *IEEE Trans. Energy Convers.*, vol. 18, no. 4, pp. 476–483, Dec. 2003.

MEHDI SAFAEIAN was born in Hamedan, Iran, in 1982. He received the B.Sc. degree from the University of Zanjan, Zanjan, Iran, in 2004, and the M.Sc. degree in electrical engineering from the Amirkabir University of Technology, Tehran, Iran, in 2007. He is currently pursuing the Ph.D. degree in electrical engineering with the University of Zanjan. His current research interests include analysis, identification, and control of electric machines, power electronics, and robust control.

ABOLFAZL JALILVAND (Member, IEEE) received the B.Sc. degree in electrical and electronic engineering from Shahid Beheshti University, Iran, in 1995, and the M.Sc. and Ph.D. degrees in power engineering and control engineering from Tabriz University, Iran, in 1998 and 2005, respectively. In 2006, he joined the Electrical Engineering Department, Zanjan University, Ira. He was promoted to Professor in 2017 .His main research interests include hybrid control systems, Petri nets, intelligent control, modeling and control of power-electronic converters, control and stabilization of power systems, and the application of intelligent methods in power systems.

ASGHAR TAHERI (Member, IEEE) was born in Zanjan, Iran, in 1977. He received the B.S. and M.S. degrees in electronics engineering from the Amirkabir University of Technology, in 1999 and 2001, respectively, and the Ph.D. degree in electronics engineering from the Iran University of Science and Technology, Tehran, Iran, in 2011. He has been a Faculty Member with the University of Zanjan, since 2010, where he was an Assistant Professor, from 2011 to 2016, and has also been an Associate Professor, since 2016. His current research interests include modeling, analysis, and control of power converters, motor drives, control, and multiphase machine drives, multilevel inverter, power electronic systems for renewable energy sources, process control, DSP and FPGA-based system designs, hardware in the loop, and computer-aided control.